Journal of ELECTRONIC MATERIALS, Vol. 43, No. 12, 2014
DOI: 10.1007/s11664-014-3395-8
© 2014 The Minerals, Metals & Materials Society

Effect of Bath Life of Ni(P) on the Brittle-Fracture Behavior of Sn-3.0Ag-0.5Cu/ENIG

WONIL SEO,[1,2] KYOUNG-HO KIM,[1] JUNG-HWAN BANG,[1] MOK-SOON KIM,[2] and SEHOON YOO[1,3,4]

1.—Welding and Joining R&BD Group, Korea Institute of Industrial Technology, Incheon 406-840, Korea. 2.—Department of Materials Science & Engineering, Inha University, Incheon 402-751, Korea. 3.—Department of Electronic Packaging Engineering, Korea University of Science and Technology, Daejeon 305-350, Korea. 4.—e-mail: yoos@kitech.re.kr

The effect of bath life of Ni(P) on the brittle-fracture behavior of Sn-3.0 wt.%Ag-0.5 wt.%Cu (SAC)/electroless nickel immersion gold (ENIG) was evaluated in this study. The bath lives of Ni(P) for the ENIG surface finish in this study were varied from 0 to 3 metal turnover (MTO), which were indirectly indicative of Ni(P) bath life, with “0 MTO” denoting the as-make-up state and “3 MTO” denoting almost waste plating solution. The SAC/ENIG sample when Ni(P) was plated in the 3 MTO bath (3 MTO sample) had thicker $(Cu,Ni)_6Sn_5$ and P-rich layers than when Ni(P) was plated in the 0 MTO bath (0 MTO sample). The brittle-fracture behavior of the 0 and 3 MTO samples was evaluated by use of a high-speed shear (HSS) test with a strain rate of 0.1–2.0 m/s. The shear strength of the 0 MTO sample was higher than that of the 3 MTO sample. The incidence of brittle fracture increased as the bath life of Ni(P) of ENIG (= MTO of Ni(P)) increased. Observation by transmission electron microscopy (TEM) revealed nano-sized voids (or particles) in the Ni-Sn-P layer. As the MTO of the Ni(P) increased, the number of nano-sized voids in the Ni-Sn-P layer of the SAC/ENIG interface increased. The poor brittle-fracture behavior of the 3 MTO sample originated from the weak interface at the thick P-rich layer and from the large nano-sized voids.

Key words: Pb-free solder, bath life, Ni(P), Sn-3.0Ag-0.5Cu, electroless nickel immersion gold, brittle fracture, high-speed shear test, interfacial microstructure

INTRODUCTION

Electroless nickel immersion gold (ENIG) has been widely adopted as a surface finish for Cu bond pads because of its effectiveness as a diffusion barrier against rapid reaction with Sn-rich solder alloys.[1,2] The structure of the intermetallic compound (IMC) layer at the interface between Sn-3.0Ag-0.5Cu (SAC) solder and ENIG is somewhat complicated; the interface is composed of $(Cu, Ni)_6Sn_5$, Ni-Sn-P, and P-rich layers (Ni_3P or Ni_2P).[3] The thickness of the Ni-Sn-P layer between the $(Cu,Ni)_6Sn_5$ and P-rich layers is approximately a few tenths of a nanometer and the Ni-Sn-P layer contains nano-voids with diameters of 10–20 nm.[4] Previous research has indicated that brittle fracture at the interface resulted from weak adhesion of the P-rich layer and/or nano-voids formed in the Ni-Sn-P layer.[5] During solder reflow, the Au of the ENIG dissolves in the molten SAC solder and then Ni(P) is exposed to the molten solder, which results in the formation of interfacial phases composed of Sn and Ni(P). Hence, the Ni(P) plating conditions affect the interfacial microstructure, which is related to the brittle-fracture behavior of the solder joints.

In this work, one of the Ni(P) plating conditions, the bath life, was varied and the microstructure of the Sn-Ag-Cu (SAC) solder joint on the ENIG surface finish was studied. The bath lives of the Ni(P)

(Received April 30, 2014; accepted August 22, 2014; published online September 13, 2014)

in this study were 0 and 3 metal turnover (MTO), which is indicative of the amount of metal added to maintain the original concentration of metal in the bath. The MTO is indirectly indicative of bath life, with "0 MTO" denoting a freshly made-up bath not supplemented with additional metal and "3 MTO" denoting three times the amount of metal in the original bath, which was almost a waste bath in our study. In industry, a long bath life (or high MTO) is very important, because it saves the make-up cost of the bath and increases the productivity of plating. However, there is no guideline of how long the plating bath can be used without leading to reliability problems after solder reflow on the Ni-based surface finish.

To understand the relationships between the bath life of the Ni(P), the ENIG surface finish, and the reliability of solder joints, the interfacial microstructure and brittle-fracture behavior of SAC solder joints on the ENIG surface finish were evaluated for different Ni(P) bath life. The brittle-fracture behavior was determined by use of a high-speed shear (HSS) tester. In addition, the SAC/ENIG interface was studied by field emission scanning electron microscopy (FE-SEM) and transmission electron microscopy (TEM).

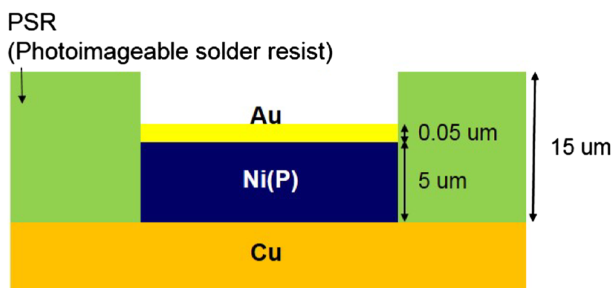

Fig. 1. Schematic diagram of the test substrate.

EXPERIMENTAL

The test printed circuit board (PCB) in this study, a solder mask-defined (SMD) type FR-4 board, is shown in Fig. 1. The diameter and thickness of the Cu pad on the test PCB were 400 μm and 10 μm, respectively. The thickness of the photoimageable solder mask (PSR) of the test PCB was 15 μm. The Cu pad was finished with ENIG. The bath life of Ni(P) of the ENIG was either 0 and 3 MTO. The concentrations of P in the Ni(P) were 6.98 wt.% and 7.74 wt.% for 0 and 3 MTO, respectively. The thickness of Ni and Au for the ENIG were 5 μm and 0.05 μm, respectively. Solder balls were then mounted on the ENIG-finished Cu pads. For solder ball mounting, Sn-3.0 wt.%Ag-0.5 wt.%Cu (SAC305) solder paste (Senju, M705-SHF) was printed on the ENIG-finished Cu pad and then a SAC305 solder ball (Ducsan Hi-Metal) of diameter 450 μm was mounted on the printed SAC305 solder paste. After mounting of the solder ball, the test PCB was reflowed in a reflow oven (Heller, 1809UL) with a peak temperature of 251°C. Figure 2 shows optical micrographs of the test sample after reflow.

The brittle-fracture behavior was evaluated by use of a high-speed shear tester (Dage, 4000HS).[6] The height of the shear tool was 50 μm from the top of the PSR on the test PCB. The shear speed (= strain rate) of the HSS test was varied from 0.1 m/s to 2.0 m/s. The shear strength was averaged for 25 samples for each condition. After the HSS test, the fracture surface was studied by optical microscopy and FE-SEM (FEI Inspect F). A cross-sectional micrograph of the joint interface was also obtained by use of the FE-SEM with energy-dispersive spectroscopy (EDS) and TEM (Jeol JEM 4010). The TEM sample was prepared with a focused ion beam (FIB, Helios 600).

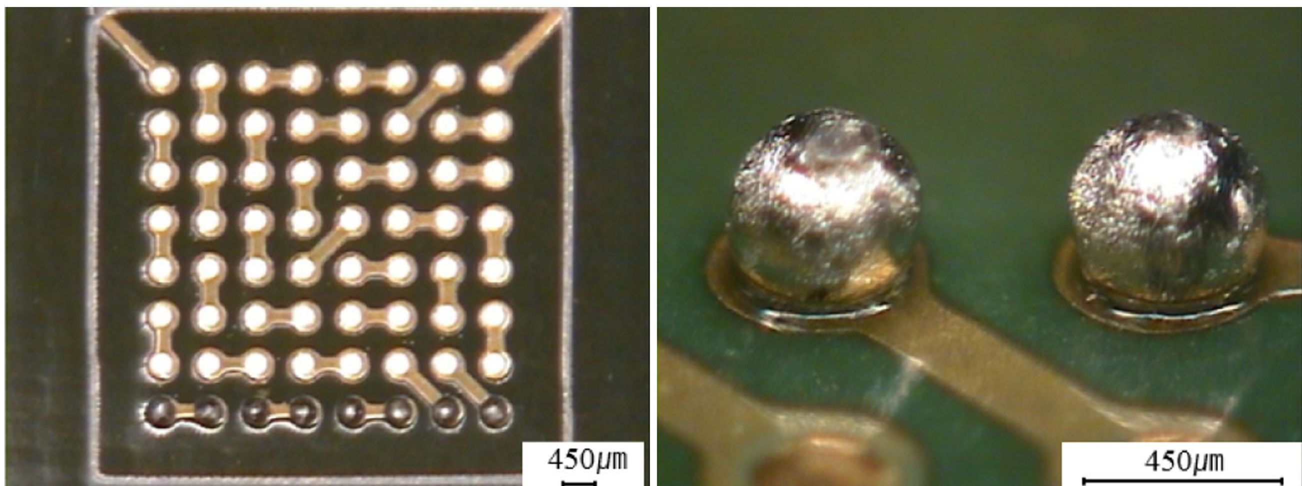

Fig. 2. Optical micrographs of the Sn-Ag-Cu solder balls on the ENIG-finished test PCB.

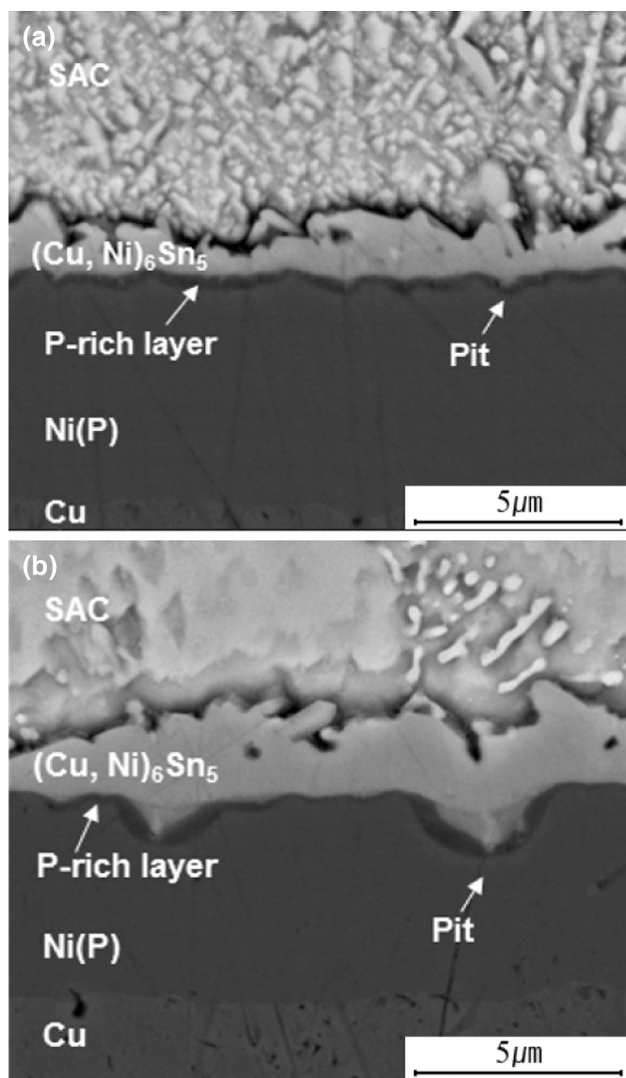

Fig. 3. Cross-sectional SEM micrographs of the SAC/ENIG showing the effect of bath life of Ni(P). The bath lives of Ni(P) were (a) 0 MTO and (b) 3 MTO.

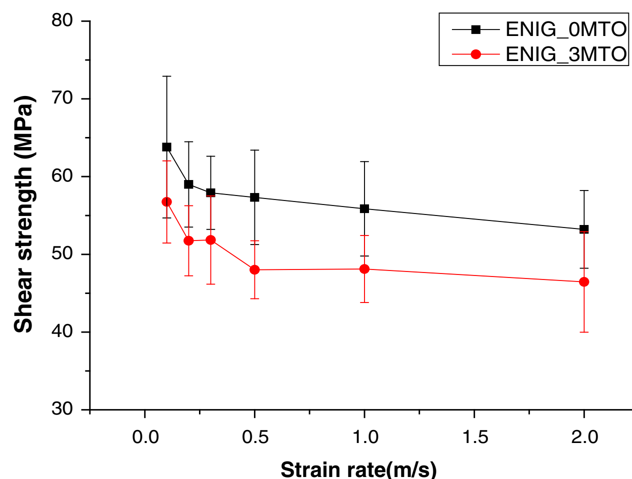

Fig. 4. Effect of bath life of Ni(P) on high-speed shear (HSS) test result for SAC/ENIG. Strain rate was varied from 0.1 to 2.0 m/s.

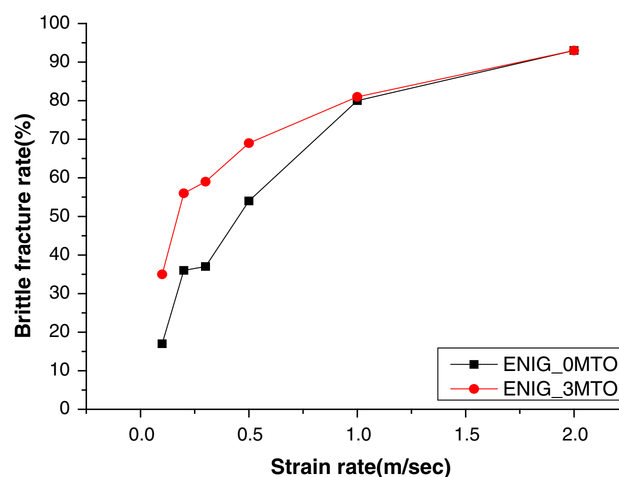

Fig. 5. Effect of varying the bath life of Ni(P) on the relationship between brittle fracture rate and strain rate for the SAC/ENIG.

RESULTS AND DISCUSSION

Figure 3 shows the cross-sectional SEM micrographs of the IMC layer for the SAC/ENIG. The bath lives of the Ni(P) of the ENIG were 0 MTO (as-make-up state) and 3 MTO (almost waste solution state). In our study, the thickness of the Au was 0.05 μm, which was thin enough to dissolve into the molten SAC solder during reflow. Therefore, no Au compound was formed in the solder matrix or at the interface. After dissolution of the Au into SAC solder, the Ni(P) was exposed to molten SAC solder, which resulted in formation of $(Cu,Ni)_6Sn_5$ at the joint interface. The thickness of the $(Cu,Ni)_6Sn_5$ layer of SAC/ENIG depended on the bath life of Ni(P) plating solution. The average thickness of the $(Cu,Ni)_6Sn_5$ layer was 1.24 μm for the 0 MTO sample (SAC/ENIG with 0 MTO Ni(P)) and 2.19 μm for the 3 MTO sample (SAC/ENIG with 3 MTO Ni(P)). Both 0 and 3 MTO samples had shallow pits at the solder joint interface and the pit size of the 3 MTO sample was larger than that of the 0 MTO sample. From area measurement by use of an image analyzer, the areas of the P-rich layer for the 0 and 3 MTO samples were 4.59 and 6.65 μm^2, respectively. Hence, the thickness of P-rich layer for the 3 MTO sample was greater than that for the 0 MTO sample. Because the P-rich layer was formed by diffusion of Ni toward the $(Cu,Ni)_6Sn_5$ IMC layer, the thickness of the P-rich layer correlated with the $(Cu,Ni)_6Sn_5$ IMC thickness, that is, the thicker P-rich layer, the greater the $(Cu,Ni)_6Sn_5$ thickness. The large thickness of the IMC and the P-rich layer of the 3 MTO sample indicated that the amount of Ni diffusion through the interface was higher for the 3 MTO sample than for the 0 MTO sample. In addition, the shallow pit region of the 3 MTO sample had a thicker P-rich layer than the other horizontal interface region. The thick P-rich layer of the pit

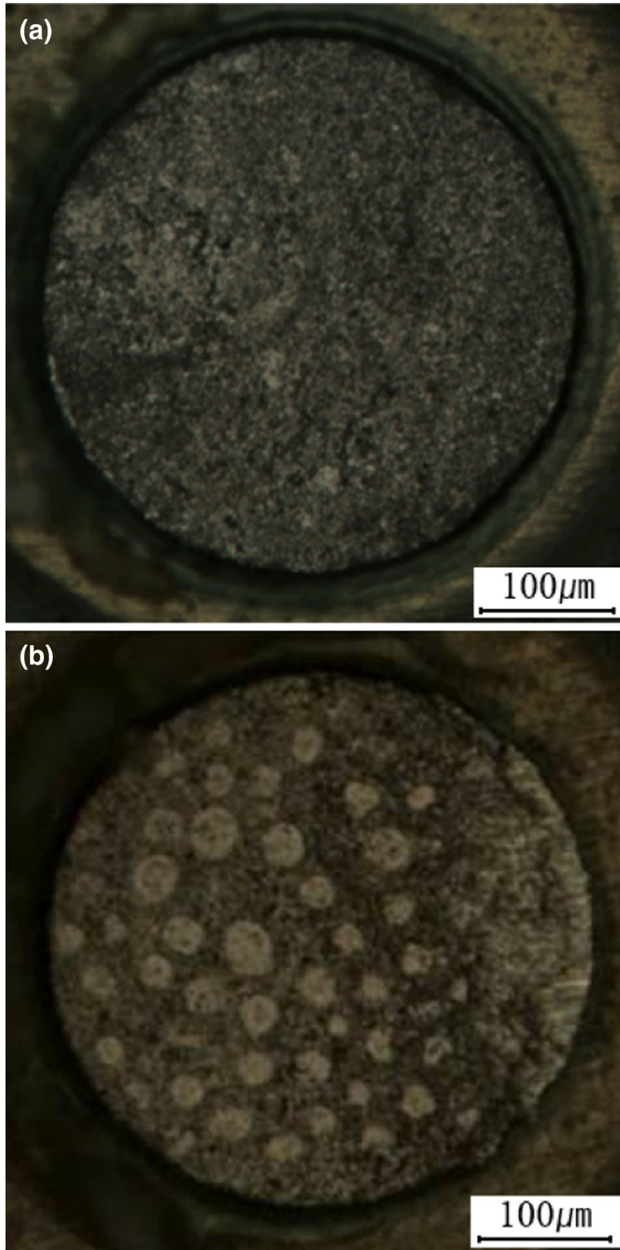

Fig. 6. Optical micrographs of the fracture surface after the HSS test for the (a) 0 MTO and (b) 3 MTO samples.

region indicated that more Ni diffusion occurred in the shallow pit region. Therefore, the shallow pits were crucial to rapid diffusion of the Ni. Because pit size was larger for the 3 MTO sample than for the 0 MTO sample, the large $(Cu,Ni)_6Sn_5$ thickness of the 3 MTO sample resulted from the rapid diffusion path of the shallow pits.

The HSS strengths of SAC/ENIG joints for different bath life (MTO) of Ni(P) were evaluated and are shown in Fig. 4. The strain rates were varied from 0.1 m/s to 2.0 m/s. The HSS strength decreased as the strain rate increased for all samples. In general, the strength of Sn-base solder increased with increasing strain rate (strain rate hardening). As the strain rate increased, solder matrix was strengthened and the fracture site moved to the "weak" IMC layer. The higher the shear speed, the more the fracture occurred at the IMC layers. Therefore, the shear strength of SAC/ENIG joints decreased with increasing shear speed. For the solder joint of the 0 MTO sample, the average shear strength was 63.8 MPa and decreased to 53.2 MPa as the strain rate was increased from 0.1 m/s to 2.0 m/s. It has been reported that the shear strength of a SAC solder joint decreased with increasing strain rate when the strain rate was higher than 0.1 m/s.[7] Sn-based solders underwent strain-rate hardening during the shear test.[8] Therefore, the failure site moved from solder to the weak IMC layers as the strain rate increased, which resulted in the decrease of shear strength with increasing strain rate. The HSS strength depended on the bath life of Ni(P). The 0 MTO samples had higher HSS strength than the 3 MTO samples. For example, the average HSS strength at 2.0 m/s was 53.2 MPa and 46.5 MPa for 0 and 3 MTO, respectively.

To understand the effect of Ni(P) bath life on the fracture behavior of SAC/ENIG, the fracture surface after the HSS test was observed by SEM. From EDS analysis, the ductile fracture surface was mainly composed of Sn and the brittle fracture surface was composed of Ni, Sn, P, and Cu, which indicated that the ductile fracture occurred in the solder region and the brittle fracture occurred at the IMC layers. In this study the fracture surface was classified into five modes (100%, 75%, 50%, 25%, and 0% brittle). The 100% brittle fracture mode indicated the entire area showed brittle fracture. The 75%, 50%, 25%, and 0% brittle fracture indicated that the percentages of the brittle fracture area on the fracture surface were 75–100%, 50–75%, 25–50%, and 0–25%. The brittle fracture rate was derived from 25 samples for each test condition. In this study, the brittle fracture rate was defined by use of the equation:

$$\text{Brittle fracture rate }(\%) = \frac{\sum(A_i \cdot N_i)}{N_{tot}} \times 100, \quad (1)$$

where A_i, N_i, and N_{tot} represent the brittle fracture variable for each brittle fracture mode, the number of samples for each brittle fracture mode, and the total number of samples, respectively. The brittle fracture variable, A_i, was 1, 0.75, 0.5, 0.25, and 0 for the 100%, 75–100%, 50–75%, 25–50%, and 0–25% brittle fracture modes, respectively. For example, the numbers of each fracture mode for the 0 MTO sample under the 0.3 m/s condition were 1, 4, 8, 5, and 7 for 100%, 75–100%, 50–75%, 25–50%, and 0–25% brittle fracture, respectively. Because the total number of samples was 25, the brittle fracture rate derived from Eq. 1 was 37.0% for the 0 MTO sample under the 0.3 m/s condition. Figure 5 shows the brittle fracture rate of the SAC solder joint on

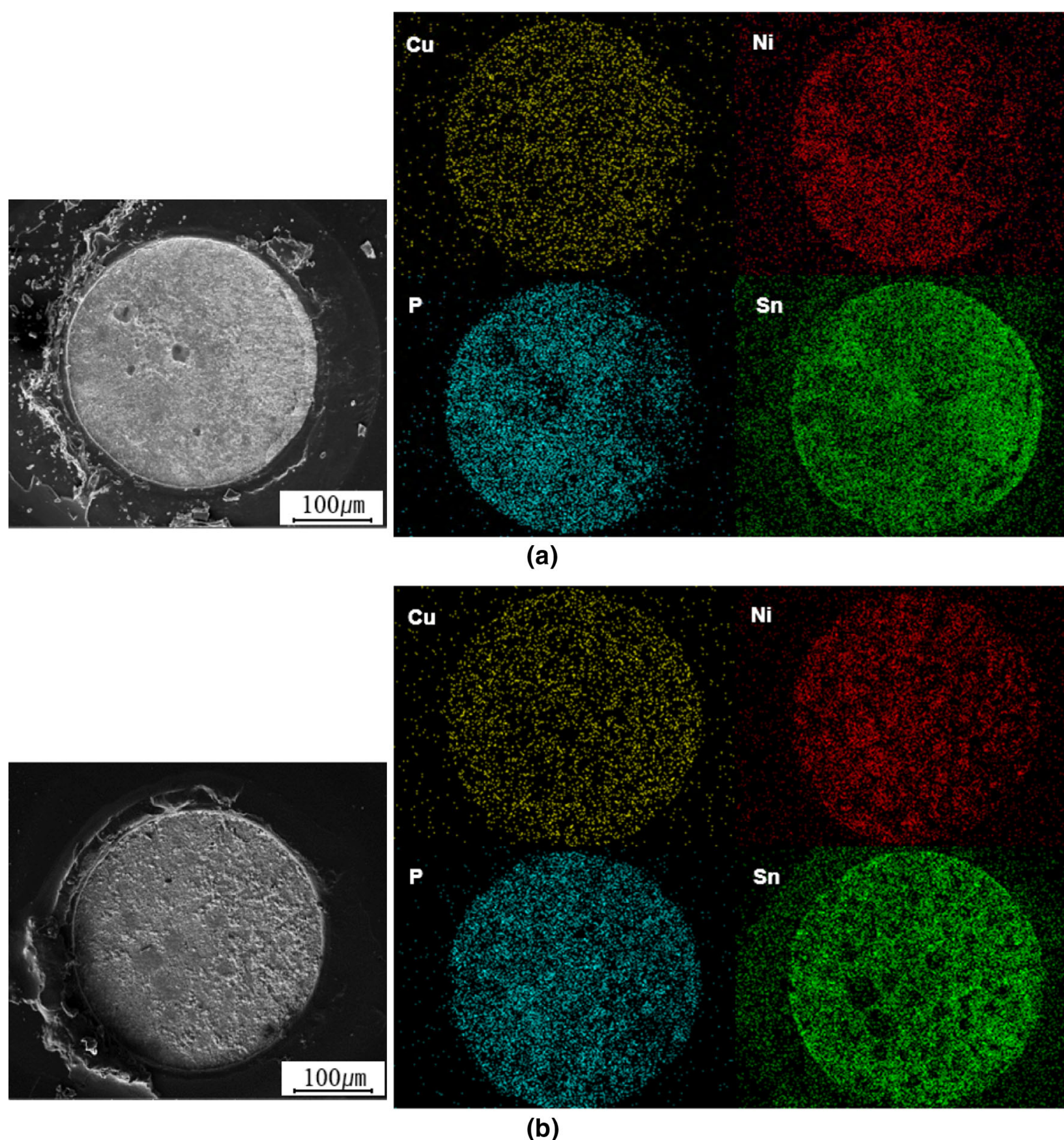

Fig. 7. SEM and EDS mapping of the fracture surface after the HSS test for the (a) 0 MTO and (b) 3 MTO samples.

ENIG (0 and 3 MTO) for different HSS test strain rate. The brittle fracture rate increased as the strain rate increased. Under 0.5 m/s strain rate, the 0 MTO samples had a lower brittle fracture rate than the 3 MTO samples. As the strain rate increases to 2.0 m/s, most samples became almost 100% brittle because of the high strain rate.

The fracture surface after the HSS test was observed by use of an optical microscope; the results are shown in Fig. 6. For the 3 MTO sample, circle-shaped features were observed on the fracture surface. We prepared another fracture surface sample and SEM with EDS mapping was conducted for the fracture surface (Fig. 7). In the EDS mapping of Sn, the circle-shaped features were clearly observed for the 3 MTO sample. In the EDS mapping image of Sn, the brightness of the circle-shaped feature was low, which indicated that the circles on the fracture surface did not contain Sn. The interfacial phase that did not contain Sn was the P-rich layer (Ni_3P). Therefore, the circle-shaped features on the fracture surface of the 3 MTO sample were the P-rich layer. Figure 8 shows cross-sectional SEM micrographs of the other fracture surface region besides the circle region. Fracture occurred mainly in the $(Cu,Ni)_6Sn_5$ IMC and at the Ni-Sn-P layer. To confirm the phase of the circle shape feature, the cross-section of the circle on the fracture surface was observed by TEM, and is shown in Fig. 9. Figure 9 shows the circle was mainly composed of a P-rich layer. The Ni-Sn-P was also observed in the cross-sectional TEM. On the circle type feature of the fracture surface, the

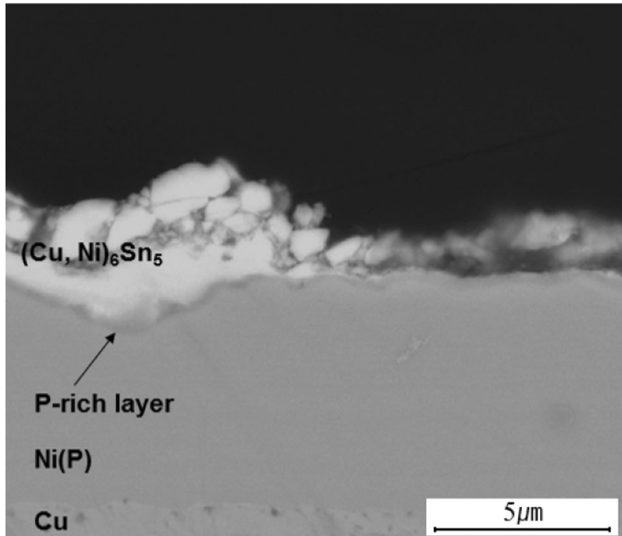

Fig. 8. Cross-sectional SEM image of the normal site on the fracture surface.

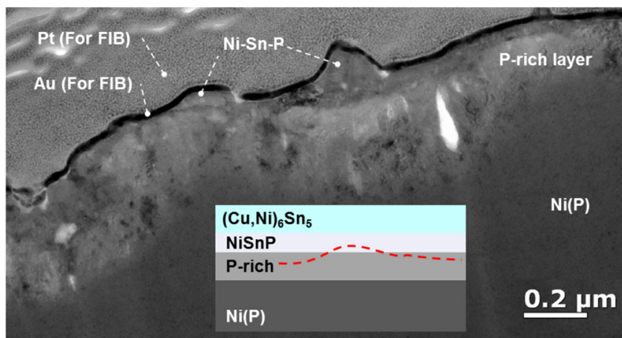

Fig. 9. Cross-sectional TEM micrographs of the circle region on the fracture surface in Fig. 6.

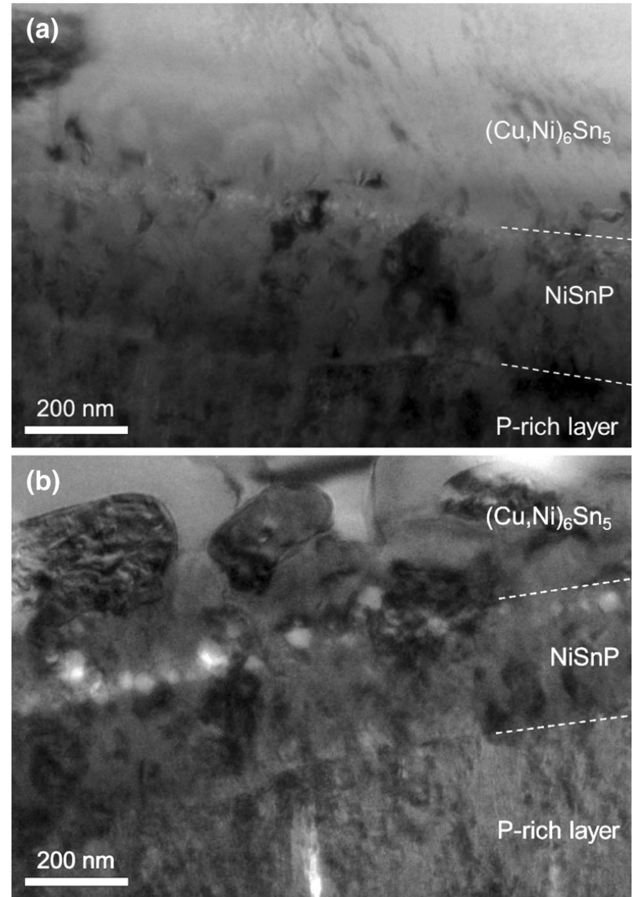

Fig. 10. Cross-sectional TEM micrographs of the NiSnP layer of the SAC/ENIG solder joint after soldering: (a) 0 MTO sample; (b) 3 MTO sample.

crack propagated mainly through the P-rich layer. The P-rich circle formation was possibly because of the thick P-rich layer of the 3 MTO sample. In summary, fracture of the 0 MTO sample occurred in $(Cu,Ni)_6Sn_5$ and Ni-Sn-P and fracture of the 3 MTO sample occurred in the P-rich layer as well as in the $(Cu,Ni)_6Sn_5$ and the Ni-Sn-P layer.

Previous workers have reported that brittle fracture at the interface resulted from the weak adhesion of the P-rich layer and/or nano-voids formed in the Ni-Sn-P layer.[5,9] To observe the nano-voids formed in the Ni-Sn-P layers of the 0 and 3 MTO samples, the interfaces of the 0 and 3 MTO samples were observed by cross-sectional TEM; the results are shown in Fig. 10. The sizes of the nano-voids in the 3 MTO sample were higher than those in the 0 MTO sample. In the 0 MTO sample, the sizes of nano-voids were approximately 5–10 nm. The sizes of the nano-voids in the 3 MTO sample were 20–40 nm. There are two mechanisms of nano-void formation. One is the Kirkendall void mechanism which results from the Sn-Ni diffusivity difference during the solder reflow process;[4,10] the other is the incorporated organic material mechanism.[3] Laurila et al.[3] reported that the nano-sized feature which appeared to be a "void" was actually organic "nanoparticles" when studied by high-resolution phase-contrast TEM. The organic nanoparticles probably originated from the Ni(P) plating bath. The plating bath for the 3 MTO sample was almost waste solution, and contained more organic contaminants than the 0 MTO sample. Hence, the Ni(P) of the 3 MTO sample had more incorporated organic matter than that of the 0 MTO sample. Therefore, the 3 MTO sample had larger "nano-voids" (actually organic nanoparticles) than the 0 MTO sample when it adopted the "organic nanoparticle" mechanism.

From our results, the 3 MTO sample had a thicker $(Cu,Ni)_6Sn_5$ and P-rich layer than the 0 MTO sample. The thick P-rich layer of the 3 MTO sample resulted in exposure of a circle-shaped, P-rich layer on the fracture surface. In addition, the 3 MTO sample contained large nano-voids (or organic nanoparticles) at the solder joint interface. Hence, the interface of the 3 MTO sample was weaker than that of the 0 MTO sample and had high brittle-fracture behavior.

CONCLUSION

The effect of the bath life of Ni(P) in ENIG on the brittle-fracture behavior of SAC solder joints was investigated in this study. After reflow, the thickness of $(Cu,Ni)_6Sn_5$ was lower for the 0 MTO sample than for the 3 MTO sample. The thickness of the P-rich layer for the 3 MTO sample was greater than that for the 0 MTO sample. After reflow of the 3 MTO sample, large shallow pits were observed at the interface between $(Cu,Ni)_6Sn_5$ and Ni(P). A thick, P-rich layer was present in the pit region of the 3 MTO sample, and the large pits of the 3 MTO sample possibly enhanced the diffusion of Ni, yielding the thick $(Cu,Ni)_6Sn_5$ layer. The brittle-fracture behavior of the 0 MTO sample was superior to that of the 3 MTO sample. During the HSS test, fracture normally occurred at several sites in the $(Cu,Ni)_6Sn_5$, Ni-Sn-P, and P-rich layers. However, a circle-shape feature was observed on the brittle fracture surface of the 3 MTO sample; this was found to be an exposed P-rich layer. The nano-voids in Ni-Sn-P layer were larger in the 3 MTO sample than in the 0 MTO sample. The weak interfacial microstructures (thick P-rich layer and large nano-voids) seemed to increase the rate of brittle fracture of the 3 MTO sample.

ACKNOWLEDGEMENTS

This work was financially supported by a research project from the Ministry of Trade, Industry and Energy, Republic of Korea.

REFERENCES

1. J. Wojewoda-Budka, Z. Huber, L. Litynska-Dobrzynska, N. Sobczak, and P. Zieba, *Mater. Chem. Phys.* 139, 276 (2013).
2. J.W. Yoon and S.B. Jung, *J. Alloy Compd.* 448, 177 (2008).
3. T. Laurila, V. Vuorinen, and J.K. Kivilahti, *Mater. Sci. Eng. R* 49, 1 (2005).
4. D. Kim and J.J. Pak, *J. Mater. Sci.: Mater. Electron.* 21, 1337 (2010).
5. K. Zeng, R. Stierman, D. Abbott, and M. Murtuza, *ITHERM'06 proceedings* (2006), pp. 1111–1119.
6. F. Song, S.W. Ricky Lee, K. Newman, B. Sykes, and S. Clark, *Proceedings of the Electronic Components and Technology Conference*, 2007, pp. 364–372.
7. K. Newman, *Proceedings of the Electronic Components and Technology Conference*, 2005, pp. 1194–1201.
8. T.T. Mattila and J.K. Kivilahti, *J. Electron. Mater.* 34, 969 (2005).
9. Y.D. Jeon, K.W. Paik, K.S. Bok, W.S. Choi, and C.L. Cho, *J. Electron. Mater.* 31, 520 (2002).
10. H.-B. Kang, J.-H. Bae, J.-W. Lee, M.-H. Park, Y.-C. Lee, J.-W. Yoon, S.-B. Jung, and C.-W. Yang, *Scrip. Mater.* 60, 257 (2009).